Journal of Solid State Chemistry **153,** 145–151 (2000)
doi:10.1006/jssc.2000.8765, available online at http://www.idealibrary.com on IDEAL®

Magnetic Properties of $Ce_{1-x}Nd_xTiO_3$ and Some Solid Solution Orthotitanates $Ln_{1-x}Ln'_xTiO_3$ (*Ln* and *Ln′* = La to Sm; $0 \leq x \leq 1$)

K. Yoshii,*,[1] A. Nakamura,† H. Abe,‡ and Y. Morii§

*Synchrotron Radiation Research Center, Japan Atomic Energy Research Institute (JAERI), Mikazuki, Hyogo 679-5148, Japan;
†Department of Materials Science, Japan Atomic Energy Research Institute (JAERI), Tokai-mura, Ibaraki 319-1195, Japan;
‡National Research Institute for Metals (NRIM), Sengen, Tsukuba, Ibaraki 305-0047, Japan; and §Advanced Science Research Center, Japan Atomic Energy Research Institute (JAERI), Tokai-mura, Ibaraki 319-1195, Japan

Received January 4, 2000; in revised form May 3, 2000; accepted May 11, 2000; published online June 29, 2000

Magnetic properties of the solid solution orthotitanate $Ce_{1-x}Nd_xTiO_3$ have been studied, where the characteristic susceptibility peaks are found in their susceptibility–temperature (χ–T) curves as in $La_{1-x}Sm_xTiO_3$ and $Pr_{1-x}Nd_xTiO_3$. The common features of this phenomenon are the pronounced magnetic hysteresis at T_P (susceptibility peak temperature), and its significant diminishment above and below T_P. The properties for some other solid solutions such as $Ce_{1-x}Sm_xTiO_3$ were also investigated. Though susceptibility peaks were found for a few of these systems, they were quite vague compared with those for the above three systems. From DC magnetization–relaxation and AC susceptibility measurements, the formation of a cluster-glass state is assumed to be a possible origin of the susceptibility peak in $Ce_{1-x}Nd_xTiO_3$, as was suggested also for $La_{1-x}Sm_xTiO_3$. Powder neutron diffraction measurements for $Ce_{0.5}Nd_{0.5}TiO_3$ revealed that neither long-range magnetic order nor structural changes exist below room temperature. The above interpretation supports this result. © 2000 Academic Press

Key Words: **orthotitanate; susceptibility peak; spin-glass; culster-glass.**

1. INTRODUCTION

The cerium titanate $CeTiO_3$ has an orthorhombic perovskite structure (space group *Pbnm*; $GdFeO_3$ type) (1–3). It is regarded as a so-called Mott–Hubbard-type insulator with a localized Ti^{3+} ($S = \frac{1}{2}$) moment on each Ti site, as is the case for the other orthotitanates $LnTiO_3$ (*Ln*: lanthanides). This moment antiferromagnetically orders at ~ 120 K with a canting angle 34°, which is denoted as the canted-antiferromagnetism (2). With decreasing temperature, its DC susceptibility–temperature (χ–T) curve shows a second upturn of susceptibility around 60 K (1, 3). This is attributed to the induced order of the Ce^{3+} ($4f^1$) localized moments, brought about by the internal field of Ti^{3+}. A DC resistivity–temperature (ρ–T) curve revealed semiconductive behavior with a band gap 0.005 eV (3).

A similar compound, $NdTiO_3$, has also the $GdFeO_3$-type structure and exhibits canted-antiferromagnetism of the Ti^{3+} moments around 90 K (4, 5). From a neutron diffraction study, it was also found that the Nd^{3+} sublattice orders magnetically at lower temperatures, induced also by the Ti^{3+} magnetic order (5). This compound also exhibits semiconductive behavior below room temperature with a band gap 0.16 eV (4). The larger band gap than that for $CeTiO_3$ is qualitatively understood in terms of a smaller 3*d* electron transfer owing to a smaller Ti^{3+}–O^{2-}–Ti^{3+} angle (6).

Physical properties of these orthotitanates have been receiving renewed attention in this decade, stimulated by the discovery of the cuprate superconductors. To see further variation of magnetic and electronic properties of these compounds, two of the present authors have recently prepared a series of solid solution orthotitanates between $CeTiO_3$ and $NdTiO_3$, $Ce_{1-x}Nd_xTiO_3$, and found characteristic susceptibility peaks in DC susceptibility–temperature (χ–T) curves (7, 8). Analogous phenomena were observed also for the orthotitanates $La_{1-x}Sm_xTiO_3$ (9) and $Pr_{1-x}Nd_xTiO_3$ (7, 8). Also for $La_{1-x}Gd_xTiO_3$ similar behavior was reported about two decades ago (10). In a subsequent work with $La_{1-x}Sm_xTiO_3$ (11), it was found that DC magnetization at 4.5 K changed almost in proportion to the logarithm of time, which is characteristic of extremely slow relaxation in magnetically frustrated systems such as spin- and cluster-glasses. Based on the absence of waiting time dependence of magnetization relaxation, i.e., aging effect, and the positive divergence of nonlinear AC susceptibilities, it was inferred that the phenomena were attributed to the formation of a cluster-glass state at low temperatures.

[1] To whom correspondence should be addressed. Tel: + 81-791-58-0892. Fax: + 81-791-58-2740. E-mail: yoshiike@spring8.or.jp.

0022-4596/00 $35.00

In this paper, we present more detailed results for $Ce_{1-x}Nd_xTiO_3$. The characteristics of this system are summarized. Based on DC magnetization–relaxation and AC susceptibility measurements, and neutron diffraction experiments, a possible origin of the susceptibility peaks is discussed. In addition, we investigated magnetic properties for some other solid solutions such as $Ce_{1-x}Sm_xTiO_3$. $SmTiO_3$ has the same $GdFeO_3$ perovskite structure and exhibits the canted-antiferromagnetism of Ti^{3+} at $T_N = 52$ K and a similar lower temperature transition at ~ 40 K to those in $CeTiO_3$ and $NdTiO_3$ (9, 12, 13).

2. EXPERIMENTAL PROCEDURES

The experimental procedures have been reported in previous papers (7–9, 11), except the following points. The systems prepared are $Ce_{1-x}Ln_xTiO_3$ with Ln = La, Pr, Nd, and Sm. The other systems containing La–Sm were prepared as well, i.e., $La_{1-x}Pr_xTiO_3$, $La_{1-x}Nd_xTiO_3$, $Ce_{1-x}Pr_xTiO_3$, and $Pr_{1-x}Sm_xTiO_3$. The x values were typically 0, 0.25, 0.5, 0.75, and 1. The y values for $Ln_{1-x}Ln'_xTiO_y$ are $3.02–3.04 \pm 0.02$ (7–9, 11).

The crystal structures were determined by the powder XRD (X-ray diffraction) method using Cu$K\alpha$ radiation (Rigaku Geigerflex). The lattice parameters were calculated from the least squares fit using the program Cell (14). The XRD patterns were assigned to an orthorhombic perovskite structure ($GdFeO_3$ type) for all the systems studied. The lattice parameters for the end compounds were confirmed to be close to those reported previously (2–5, 12, 13). For all the systems, they exhibited comparably smooth changes with x, as was shown for $Ce_{1-x}Nd_xTiO_3$, $Pr_{1-x}Nd_xTiO_3$, and $La_{1-x}Sm_xTiO_3$ (7, 9). In $La_{1-x}Sm_xTiO_3$, composition dependence of all the lattice parameters occurs around $x \sim 0.3$, below which the susceptibility peak is clearly found (9), suggesting the relationship between the peak and the crystal structure. Such a correlation was not obviously found in the present systems.

DC magnetization measurements were carried out using a SQUID magnetometer (Quantum Design MPMS). DC susceptibility–temperature (χ–T) curves were measured in the FC (field-cooled) and RM (remanent magnetization) conditions between 4.5 and 300 K. The former was measured in a cooling run with an applied field (**H**) of 100 Oe. The latter was measured in a heating run after zero field cooling to 4.5 K, applying an **H** = 55,000 Oe field and then reducing it to 100 Oe. DC magnetization–magnetic field (**M**–**H**) isotherm curves were measured at several temperatures within the field $\pm$ 55,000 Oe. Relaxation of magnetization was measured at 4.5 K as a function of time (t) with a field (**H**) up to 100 Oe. AC susceptibility–temperature ($\chi(\omega)$–T) curves were measured using a Quantum Design PPMS. DC resistivity–temperature (ρ–T) curve measurements were carried out by the conventional four-probe technique below room temperature.

Powder neutron diffraction data were measured for $Ce_{0.5}Nd_{0.5}TiO_3$ with a high-resolution powder diffractometer (HRPD) at the JRR-3M reactor of JAERI with a neutron wavelength $\lambda = 1.1624$ Å using a Si(5 3 1) monochromator. The experiments were carried out at room temperature, 50 K, 90 K, and 10 K with a diffraction angle 2θ between 5 and 165°, and an angle step 0.05°. The patterns obtained were fitted in a 2θ range between 10 and 120° by the Rietveld method using the program RIETAN (15).

3. RESULTS AND DISCUSSION

3.1. DC Susceptibility Data

Figure 1 summarizes the DC magnetic measurements of $Ce_{1-x}Nd_xTiO_3$. The profiles and the transition temperatures obtained from DC susceptibility–temperature (χ–T) curves of $CeTiO_3$ ($x = 0$) and $NdTiO_3$ ($x = 1$) in Fig. 1 are close to those in the previous results: T_N (Neel temperature) ~ 120 K and T_{N2} (Ce^{3+} ordering temperature) $\sim$ 60–80 K for $CeTiO_3$ (1–3), and $T_N \sim 90$ K for $NdTiO_3$ (4,5). Their RM susceptibilities were typically $\sim 20\%$ larger than the FC susceptibilities below T_N for $CeTiO_3$ but ~ 3.5 times smaller for $NdTiO_3$. The lower T_N of $NdTiO_3$ is explained in terms of the weakening of exchange interactions, arising from the decrease of a Ti^{3+}–O^{2-}–Ti^{3+} angle caused by the larger orthorhombic distortion (11).

The figure shows also that the solid solution compounds show drastic alternation of the χ–T curves, resulting in the susceptibility peaks for the Nd substitution (x) ≥ 0.5. The characteristics in this figure are summarized as follows:

(1) Each curve exhibits a similar transition at T_N with rapid increase of susceptibility between 90 and 110 K to those for the end compounds. The value of T_N decreases monotonously with increasing x, which is understood in terms of the decrease of an average Ti^{3+}–O^{2-}–Ti^{3+} angle.

(2) Each curve with $0.5 \leq x \leq 0.75$ shows a characteristic susceptibility peak around 20–60 K (peak temperature, T_P). The susceptibility decreases again below ~ 30 K (T'_N) typically to $\sim 1/20$ compared to that at T_P (peak susceptibility, χ_P). T_P slightly increases with increasing x.

(3) The FC susceptibilities are typically $\sim 20\%$ larger than those of RM around T_P, which is different from the behavior of simple ferromagnetism. The antiferromagnetic Weiss constants obtained (around-100 K) from the Curie–Weiss fit imply the order at T_P is due to remaining canted-antiferromagnetism.

(4) Magnetic hysteresis loops with residual magnetization are the most pronounced at T_P, elucidated from the **M**–**H** curve measurements (7). Below T_N, **M**–**H** curves exhibited comparably linear slopes with no saturation magnetization, and their residual moments were generally $\sim 1/10$ compared to those at T_P.

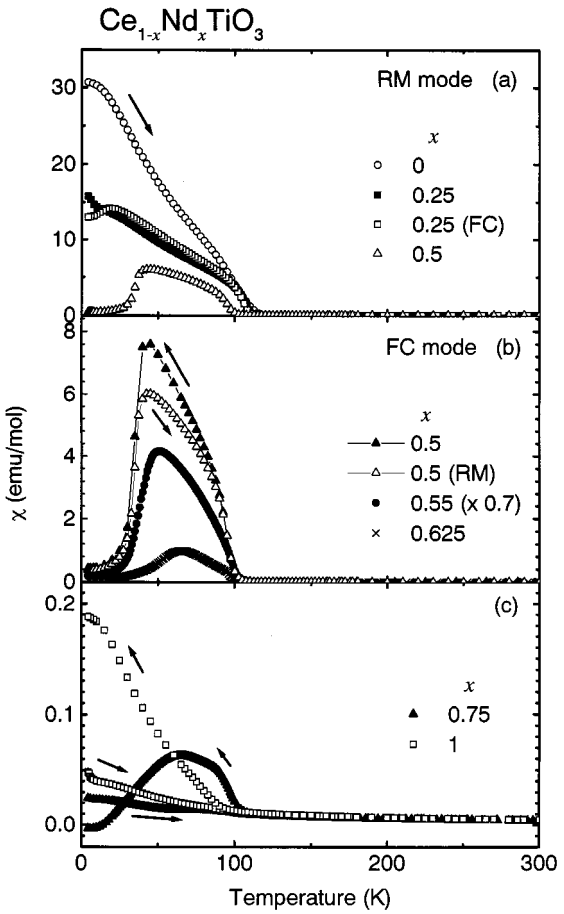

FIG. 1. (a) DC susceptibility–temperature (χ–T) curves for $Ce_{1-x}Nd_xTiO_3$ with $x = 0$, 0.25, and 0.5, measured in RM condition. For $x = 0.25$, an FC curve is also shown. (b) The same as (a) for $x = 0.5$, 0.55, and 0.625, measured in FC condition. For $x = 0.5$, an RM curve is also shown. (c) The same as (a) for $x = 0.75$ and 1. The susceptibilities of $x = 0.55$ are multiplied by a factor of 0.7. The arrows, $\leftarrow$ and $\rightarrow$, stand for the FC and RM conditions, respectively.

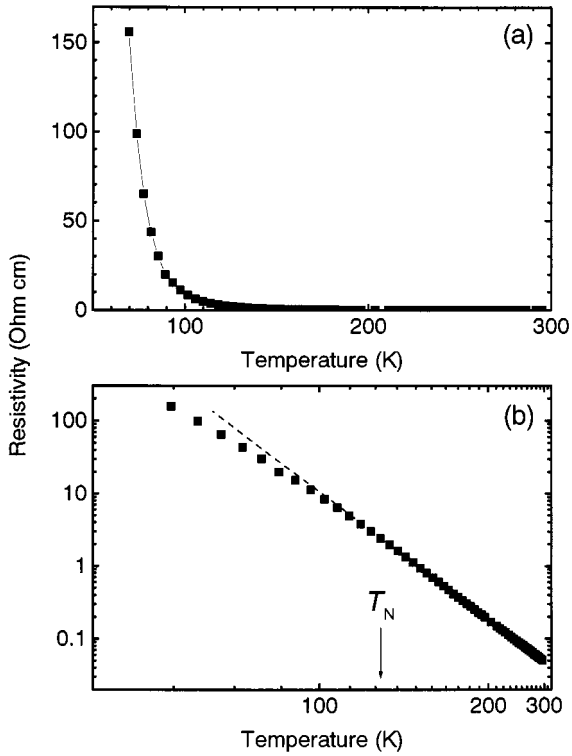

FIG. 2. DC resistivity–temperature (ρ–T) curve for $Ce_{0.5}Nd_{0.5}TiO_3$ in (a) linear scale and (b) $\log_{10}\rho$–$1/T$ scale. A dotted line in (b) represents a semiconductive curve with a band gap ~ 0.07 eV.

Figure 2 shows a DC resistivity–temperature (ρ–T) curve for $x = 0.5$, which shows the most pronounced susceptibility peaks among all the systems. Figure 2a reveals semiconductive behavior below 300 K. The band gap was calculated to be ~ 0.07 eV. Thus the system is regarded as a Mott–Hubbard insulator like the end compounds. It is reasonable that the band gap is between those of $CeTiO_3$ (0.005 eV (3)) and $NdTiO_3$ (0.16 eV (4)), considering that the Ti3d electron transfer is governed by the average Ti^{3+}–O^{2-}–Ti^{3+} angle. Figure 2b shows slight change of temperature dependence of ρ around T_N (= 122 K). This may indicate the decrease of random electron scattering, owing to the canted-antiferromagnetism. Unfortunately, precise measurements could not be carried out below ~ 60 K because of large resistance values.

These results shows that the canted-antiferromagnetic order similar to that in the end compounds remains around T_N in the solid solutions. This order, however, is drastically modified by the Nd substitution of 50% below T_P, leading to the characteristic susceptibility peaks. For comparison, DC magnetic data for one of the other similar solid solutions, $Ce_{1-x}Sm_xTiO_3$, are shown in Figs. 3a and 3b. As the RM susceptibilities were typically $\sim 20\%$ larger than those of FC for most of the systems, experimental data are shown mainly for the former condition. The FC and RM curves are of analogous shapes for the systems other than $x = 0.9$. Figure 3b indicates that the large amounts of the Sm substitution of $x = 0.75$ and 0.9 cause the considerable modification of the canted-antiferromagnetism, leading to the susceptibility peaks around 10 K, though the peaks are vague compared with those in $Ce_{1-x}Nd_xTiO_3$.

Figures 4a and 4b show **M**–**H** curves for some representative $Ce_{1-x}Sm_xTiO_3$ samples measured at 4.5 K. The value of saturation magnetization for $CeTiO_3$ is close to that in Ref. (1). Figure 4a represents gradual decrease of the values of coercivity and residual magnetization by the Sm substitution, both of which were foundto change almost linearly for $x \leq 0.75$. Figure 4b shows the different profiles of the **M**–**H** curves with small hysteresis for $x = 0.9$. The results in Figs. 3 and 4

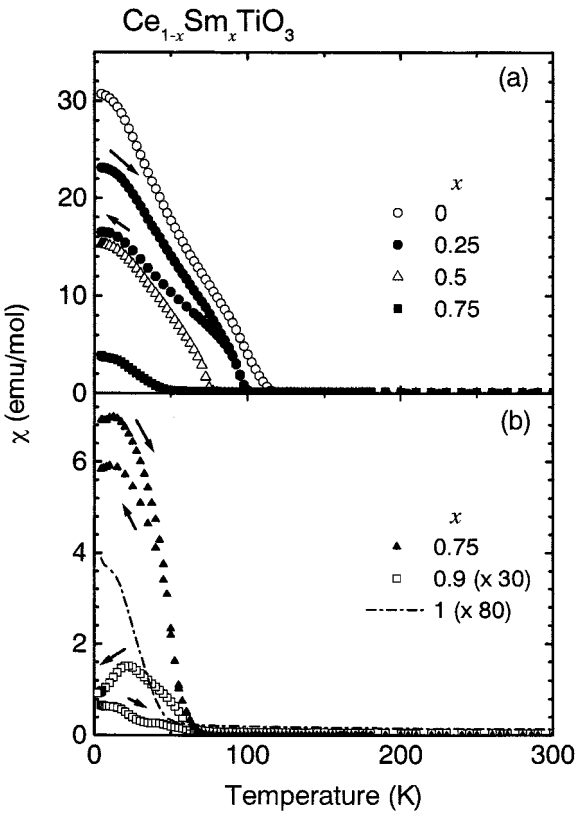

FIG. 3. χ–T curves for $Ce_{1-x}Sm_xTiO_3$ with (a) $x = 0$, 0.25, 0.5, and 0.75, and (b) $x = 0.75$, 0.9, and 1, which were measured in RM condition. For $x = 0.25$, 0.75, and 0.9, also FC curves are shown. The susceptibilities for $x = 0.9$ and 1 are multiplied by factors of 30 and 80, respectively. The meaning of the arrows is as in Fig. 1.

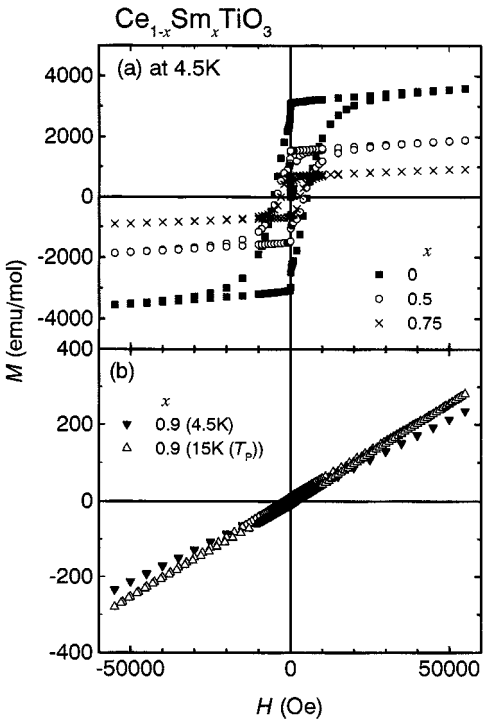

FIG. 4. (a) **M**–**H** curves for $Ce_{1-x}Sm_xTiO_3$ with (a) $x = 0$, 0.5, and 0.75 at 4.5 K, and (b) $x = 0.9$ at 4.5 and 15 K (around T_P).

indicate that, despite the significant modification of magnetic structures around $x = 0.75$–0.9, the magnetic properties at low temperatures seem to be well scaled against the Ce content $(1 - x)$ in most of the x region, which is a considerably different nature from those of $Ce_{1-x}Nd_xTiO_3$. Quite similar results have also been obtained for $Pr_{1-x}Sm_xTiO_3$, as is seen in Fig. 5. For the other systems studied, the susceptibility peak has not yet been clearly found. Their χ–T curves showed similar profiles to those of the end compounds.

Apparently the details of the properties are different in each system. They were pointed out in Ref. (11) among the systems $Ce_{1-x}Nd_xTiO_3$, $La_{1-x}Sm_xTiO_3$, and $Pr_{1-x}Nd_xTiO_3$. Comparing the data for $Ce_{1-x}Ln_xTiO_3$ and $Pr_{1-x}Ln_xTiO_3$ with $Ln = Nd$ and Sm, it is common that the distinct susceptibility peaks are found only in the case of $Ln = Nd$. In addition, the χ–T curves of $Ce_{1-x}Sm_xTiO_3$ and $Pr_{1-x}Sm_xTiO_3$ have similar profiles (Figs. 3 and 5). These facts suggest that different commitment of the lanthanide ions in magnetic interactions plays important role. Their details are to be clarified in future.

3.2. DC Magnetization–Relaxation, AC Susceptibility, and Neutron Diffraction Data

As was noted earlier, for $La_{1-x}Sm_xTiO_3$ (11), DC magnetization–relaxation and AC susceptibility measurements were performed considering the susceptibility peak in $La_{1-x}Gd_xTiO_3$ (10) whose origin was speculated as a spin-glass. A possible origin of the decrease of magnetization below T_P in $La_{1-x}Sm_xTiO_3$ was assumed to be a similar magnetic state denoted as a cluster-glass, i.e., freezing of random orientation of ferromagnetically ordered clusters. The present results might also be explained in this context, as the randomness of plausible magnetic interactions exists because of the solid solution formation. The existence of a magnetically random state seems consistent with the deviation between the FC and RM curves below T_N, indicating the irreversible nature of the phenomena. In this work, these experiments were carried out for $Ce_{0.5}Nd_{0.5}TiO_3$, which showed the largest susceptibility peaks.

Figure 6 shows magnetization plotted against time (t) for $Ce_{0.5}Nd_{0.5}TiO_3$, measured at 4.5 K. The curve (a) was measured as follows. The sample was zero-field-cooled down to 4.5 K, and then it was maintained for a waiting time $t_w = 0$ (min) before the application of the 50 Oe field (**H**). As soon as the field was applied, magnetization was measured as a function of time. The curve (b) was measured in the same manner except for $t_W = 50$ min and

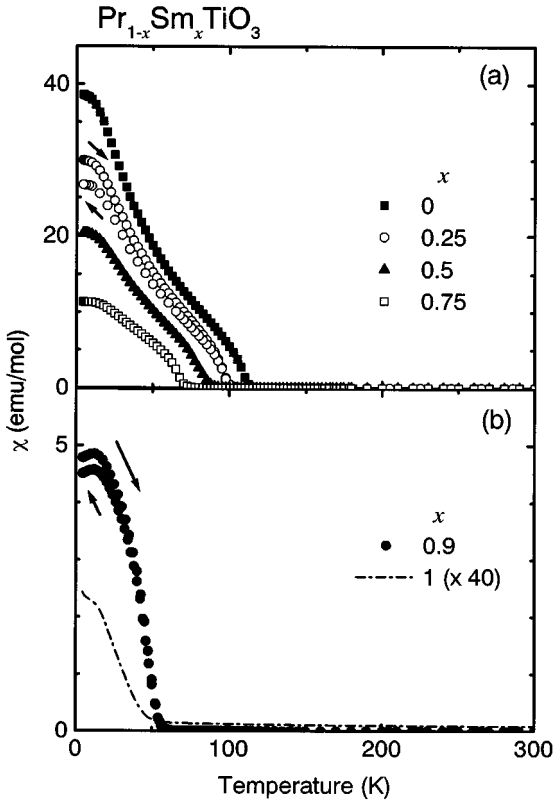

FIG. 5. χ–T curves for $Pr_{1-x}Sm_xTiO_3$ with (a) $x = 0$, 0.25, 0.5, and 0.75, and (b) $x = 0.9$ and 1, which were measured in RM condition. For $x = 0.25$ and 0.9, also FC curves are shown. The meaning of the arrows is as in Fig. 1. The susceptibilities for $x = 1$ are multiplied by a factor of 40.

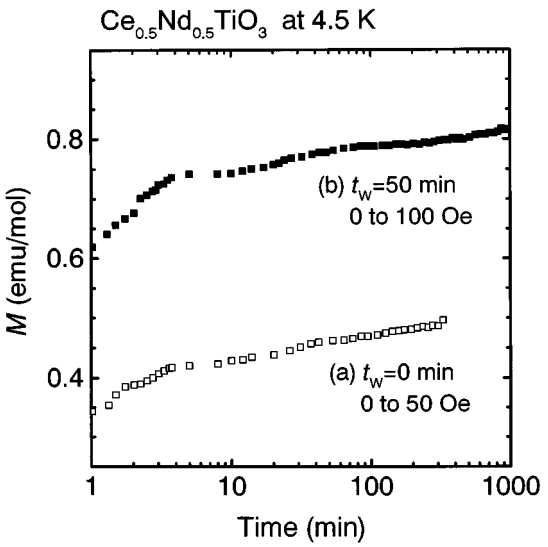

FIG. 6. Magnetization (**M**) plotted against time (t) curves for $Ce_{0.5}Nd_{0.5}TiO_3$ measured at 4.5 K. See text for more details.

H = 100 Oe. Although there exists some fluctuation in each curve, magnetization tends to change linearly with the logarithm of time. This is a typical feature for extremely slow relaxation processes in magnetically frustrated systems such as spin- and cluster-glasses below the freezing temperature, T_g (16, 17). For the spin-glass phenomenon, another feature called the aging effect (17) is observed below T_g. Namely, the value of **M** shows a change of time dependence around the waiting time t_w. No such phenomenon is clearly observed in the figure. The inflection in both curves around $t \sim 3$ min has no correlation with t_w. These results are true also for the experiments with different combinations of the t_w and **H** values.

Figures 7a and 7b show AC susceptibility–temperature ($\chi(\omega)$–T) curves for $Ce_{0.5}Nd_{0.5}TiO_3$, measured in cooling from 300 K. Figure 7a exhibits the maximums of a linear susceptibility $\chi_0(\omega)$ around 80–100 and 35 K, which are slightly lower than $T_N = 110$ K and $T_P = 45$ K, respectively. Such maxima are ascribed to magnetic phase transitions (including spin- and cluster-glass transitions). Figure 7b shows that the value of $(\frac{3}{4})\chi_2(\omega)h^2$, corresponding to the third-order susceptibility (18), exhibits a broad peak with a positive sign around 80–100 K. A very small peak with a positive sign ($\sim 6 \times 10^{-5}$ emu/mol) was also observed slightly above T_P ($\sim$ 53 K), which is not clearly seen in the figure. These are just reverse of the behavior for a spin-glass where $(\frac{3}{4})\chi_2(\omega)h^2$ negatively diverges at the freezing temperature (18). The results of Figs. 6 and 7, representing slow relaxation processes other than a spin-glass, are qualitatively the same as those obtained for $La_{1-x}Sm_xTiO_3$. Thus the origin of the susceptibility peak in $Ce_{1-x}Nd_xTiO_3$ might be the formation of a cluster-glass.

Figure 8 shows a neutron diffraction pattern at 50 K (near T_P) for $Ce_{0.5}Nd_{0.5}TiO_3$, whose profile quite resembles those of $CeTiO_3$ (2) and $NdTiO_3$ (5) above T_N. For these end compounds, several magnetic Bragg peaks were observed below T_N for 2θ less than $\sim 40^\circ$ due to the canted-antiferromagnetism of the Ti^{3+} sublattice and the induced ordering of the lanthanide sublattices (2, 5). However, no such a peak was observed in the whole angle region. Indeed this pattern could be suitably fitted to the orthorhombic $GdFeO_3$ structure (space group *Pbnm*), assuming that all the peaks are nuclear Bragg peaks. Reliability (R) factors are $R_{WP} = 7.73\%$, $R_I = 3.80\%$, and $R_F = 2.21\%$. The lattice parameters are $a = 5.5562(2)$ Å, $b = 5.5938(2)$ Å, and $c = 7.8140(3)$ Å. Their deviation from the values in Ref. (7) might be due to the difference of oxygen contents within the experimental error. The fractional coordinates were essentially identical as those for $CeTiO_3$ (2) and $NdTiO_3$ (5). Isotropic thermal parameters (B) were 0.1–0.2 $Å^2$.

The patterns taken at room temperature, 90 K, and 10 K showed almost identical profiles to that in the figure. They could be well fitted also with the same *Pbnm* symmetry and nearly the same parameters and reliability factors. These results elucidate the lack of long-range magnetic order even around T_P. Therefore, the largest hysteresis loop near T_P in the **M**–**H** curve originates from short-range magnetic order.

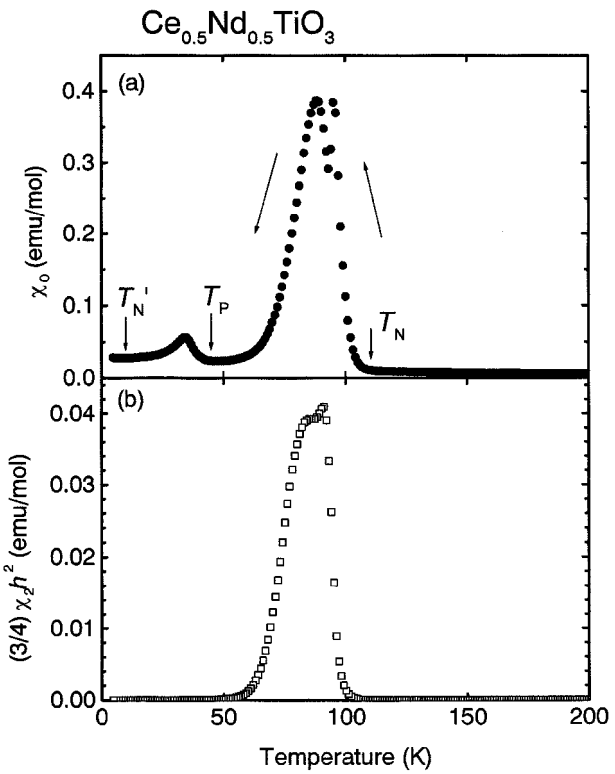

FIG. 7. AC susceptibility–temperature ($\chi(\omega)$–T) curves for $Ce_{0.5}Nd_{0.5}TiO_3$. (a) $\chi_0(\omega)$ and (b) $(\frac{3}{4})\chi_2(\omega)h^2$ values plotted against temperature measured with cooling the sample, where $\chi_0(\omega)$, $\chi_2(\omega)$, ω, and h stand for linear susceptibility, third-order susceptibility (18), frequency of the applied AC field (1000 Hz), and strength of the AC field (10 Oe), respectively.

The formation of a cluster-glass below T_P seems to be consistent with the results.

It is noteworthy that qualitatively the same result was also obtained from the powder neutron diffraction measurements for $La_{1-x}Sm_xTiO_3$. Although no quantitative analysis could be carried out because of quite poor intensities caused by strong neutron absorption of Sm, neither a magnetic Bragg peak nor a change of the profile of the pattern was observed below T_N. This suggests that the susceptibility peaks are commonly interpreted in terms of a cluster-glass.

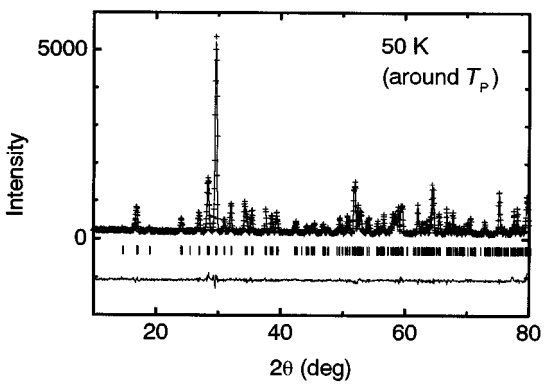

FIG. 8. Neutron diffraction patterns with a 2θ range between 10 and 80° at 50 K (around T_P). The observed and calculated patterns are shown with " + " and the top solid line, respectively. The vertical markers stand for the angles of Bragg reflections. The lowest solid lines represent the difference between the calculated and observed intensities. See text for more details.

4. SUMMARY

Magnetic properties of the solid solution orthotitanate $Ce_{1-x}Nd_xTiO_3$ have been studied, where the characteristic susceptibility peaks were found in their χ–T curves as in $La_{1-x}Sm_xTiO_3$ and $Pr_{1-x}Nd_xTiO_3$. The common features of this phenomenon are the most pronounced magnetic hysteresis at T_P (susceptibility peak temperature) and its significant loss above and below T_P. Though susceptibility peaks were found for several other systems, they were quite vague compared with those for the three systems above.

From DC magnetization–relaxation and AC susceptibility measurements, the formation of a cluster-glass state is assumed to be a possible origin of the susceptibility peak in $Ce_{1-x}Nd_xTiO_3$, as was suggested also for $La_{1-x}Sm_xTiO_3$. Powder neutron diffraction measurements for $Ce_{0.5}Nd_{0.5}TiO_3$ revealed that neither long-range magnetic order nor structural changes exist below room temperature. The interpretation above supports the result.

ACKNOWLEDGMENTS

The authors gratefully thank Mr. Y. Shimojo and Dr. S. Okayasu of JAERI for their support in performing the neutron diffraction and AC susceptibility measurements, respectively. Dr. T. Inami of JAERI is also greatly acknowledged for his help in the neutron diffraction data analyses.

REFERENCES

1. D. A. MacLean and J. E. Greedan, *Inorg. Chem.* **20,** 1025 (1981).
2. J. P. Goral and J. E. Greedan, *J. Magn. Magn. Mater.* **37,** 315 (1983).
3. J. E. Sunstrom IV, S. M. Kauzlarich, and M. R. Antonio, *Chem. Mater.* **5,** 182 (1993).
4. C. Eylem, H. L. Ju, B. W. Eichhorn, and R. L. Greene, *J. Solid State Chem.* **114,** 164 (1995).
5. G. Amow and J. E. Greedan, *J. Solid State Chem.* **121,** 443 (1996).
6. Y. Taguchi, Y. Tokura, T. Arima, and F. Inaba, *Phys. Rev. B* **48,** 511 (1993).
7. K. Yoshii and A. Nakamura, *J. Solid State Chem.* **137,** 181 (1998).
8. K. Yoshii and A. Nakamura, *Physica B* **259–261,** 900 (1999).
9. K. Yoshii and A. Nakamura, *J. Solid State Chem.* **133,** 584 (1997).
10. J. P. Goral and J. E. Greedan, *J. Solid State Chem.* **43,** 204 (1982).
11. K. Yoshii, A. Nakamura, and H. Abe, *J. Alloys Compd.* **290,** 236 (1999).
12. D. A. MacLean, H.-N. Ng, and J. E. Greedan, *J. Solid State Chem.* **30,** 35 (1979).
13. G. Amow, J. E. Greedan, and C. Ritter, *J. Solid State Chem.* **141,** 262 (1998).

14. Y. Takaki, T. Taniguchi, H. Yamaguchi, and K. Nakata, *J. Ceram. Soc. Jpn., Int. Ed.* **96,** 13 (1988).
15. (a) F. Izumi, *in* "The Rietveld method" (R. A. Young, Ed.), Chap. 13. Oxford Univ. Press, Oxford, 1993. (b) Y.-I. Kim and F. Izumi, *J. Ceram. Soc. Jpn.* **102,** 401 (1994).
16. K. Binder and A. P. Young, *Rev. Mod. Phys.* **58,** 801 (1986).
17. M. Itoh, I. Natori, S. Kubota, and K. Motoya, *J. Phys. Soc. Jpn.* **63,** 1486 (1994).
18. S. Chikazawa, T. Saito, T. Sato, and Y. Miyako, *J. Phys. Soc. Jpn.* **47,** 335 (1979). T. Taniguchi, H. Matsuyama, S. Chikazawa, and Y. Miyako, *J. Phys. Soc. Jpn.* **52,** 4323 (1983).